Open access • Journal Article • DOI:10.1002/2014JD022249

Quantifying the heat flux regulation of metropolitan land use/land cover components by coupling remote sensing modeling with in situ measurement — Source link

Wenhui Kuang, Yinyin Dou, Chi Zhang, Chi Zhang ...+5 more authors

Institutions: Chinese Academy of Sciences, Beijing Normal University, Hubei University

Published on: 16 Jan 2015 - Journal of Geophysical Research (John Wiley & Sons, Ltd)

Topics: Bowen ratio, Sensible heat, Urban heat island, Latent heat and Land cover

AGU PUBLICATIONS

JGR

Journal of Geophysical Research: Atmospheres

RESEARCH ARTICLE
10.1002/2014JD022249

Key Points:
- A calibration method reduced uncertainty due to subjective judgment of parameter
- High-rise resident area is cooler than lower rise area
- Heat-dissipating strength of vegetation declined exponentially with its coverage

Supporting Information:
- Readme
- Figures S1–S3

Correspondence to:
C. Zhang,
zc@ms.xjb.ac.cn

Citation:
Kuang, W., Y. Dou, C. Zhang, W. Chi, A. Liu, Y. Liu, R. Zhang, and J. Liu (2015), Quantifying the heat flux regulation of metropolitan land use/land cover components by coupling remote sensing modeling with in situ measurement, *J. Geophys. Res. Atmos.*, *120*, 113–130, doi:10.1002/2014JD022249.

Received 4 JUL 2014
Accepted 4 DEC 2014
Accepted article online 8 DEC 2014
Published online 12 JAN 2015

Quantifying the heat flux regulation of metropolitan land use/land cover components by coupling remote sensing modeling with in situ measurement

Wenhui Kuang[1], Yinyin Dou[2], Chi Zhang[3,4], Wenfeng Chi[1,5], Ailin Liu[1,5], Yue Liu[1], Renhua Zhang[1], and Jiyuan Liu[1]

[1]Key Laboratory of Land Surface Pattern and Simulation, Institute of Geographic Sciences and Natural Resources Research, Chinese Academy of Sciences, Beijing, China, [2]Center for Human-Environment System Sustainability, Beijing Normal University, Beijing, China, [3]State Key Laboratory of Desert and Oasis Ecology, Xinjiang Institute of Ecology and Geography, Chinese Academy of Sciences, Urumqi, China, [4]School of Resources Environment Science and Engineering, Hubei University of Science and Technology, Hubei, China, [5]College of Resources and Environment, University of Chinese Academy of Sciences, Beijing, China

Abstract Quantifying the effects of urban land use/land cover with regard to surface radiation and heat flux regulation is important to ecological planning and heat stress mitigation. To retrieve the spatial pattern of heat fluxes in the Beijing metropolitan area, China, a remote sensing-based energy balance model was calibrated with synchronously measured energy fluxes including net radiation, latent heat flux (LE), and sensible heat flux (H). Our model calibration approach avoided the uncertainties due to subjective judgments in previous empirical parameterization methods. The land surface temperature (LST), H, and Bowen ratio (β) of Beijing were found to increase along the outskirt-suburban-urban gradient, with strong spatial variation. LST and H were negatively correlated with vegetation fraction cover (VFC). For example, the modern high-rise residential areas with relatively higher VFC had lower H and β than the traditional low-rise residential areas. Our findings that indicate thermal dissipation through vegetation transpiration might play an important role in urban heat regulation. Notably, the thermal dissipating strength of vegetation (calculated as LE/VFC) declined exponentially with increased VFC. For the purpose of heat stress regulation, we recommend upgrading the traditional low-rise residential areas to modern high-rise residential areas and focusing urban greenery projects in areas whose VFC < 0.1, where the heat regulating service by urban vegetation could be twice as effective as in other places.

1. Introduction

In the context of global warming, the increase of urban heat island (UHI) intensity not only severely affects the local comfort of urban residents, human health, and energy consumption [*Laaidi et al.*, 2012; *Vandentorren et al.*, 2006] but also changes the global radiation, heat flux, moisture flux, and the balance of Earth's hydrological system [*Owen et al.*, 1998; *Kalnay and Cai*, 2003; *Grimmond*, 2007; *Grimm et al.*, 2008; *Mirzaei and Haghighat*, 2010; *Seto et al.*, 2012]. UHI is primarily related to the altered land surface structure and energy exchange process due to urbanization, which result in special atmospheric circulation and energy partition patterns that enhance sensible heat flux (H) in urbanized areas [*Arnfield*, 2003; *Imhoff et al.*, 2010]. Ignoring the relatively small anthropogenic energy release [*Chen et al.*, 2012], energy balance for urban land may be written as

$$R_n = H + \mathrm{LE} + G \tag{1}$$

where R_n is net radiation, LE is latent heat, and G is the (primarily) conductive heat flux into or out of the material that constitutes the surface. For certain R_n and G (G is correlated to R_n), the less energy dissipated as LE (through evapotranspiration), the higher H and temperature, and vice versa. Urban lands are covered by large areas of impervious surfaces, which reduce the evaporative sink, leading to high Bowen ratio $\left(\beta = \frac{H}{\mathrm{LE}}\right)$ and increased surface temperature in intensively developed areas, even at night [*Asaeda and Ca*, 1993; *Owen et al.*, 1998; *Xiao et al.*, 2007; *Weng and Lu*, 2008; *Y. Zhang et al.*, 2009; *Liu et al.*, 2012a, 2012b; *Mallick et al.*, 2013]. In contrast, the urban green spaces have strong evapotranspiration compared to moist rural ecosystems and are effective in suppressing surface heat by dissipating energy through LE [*Suckling*, 1980; *Cao et al.*, 2010; *Imhoff et al.*, 2010]. Obviously, different land use/land cover (LULC) types have distinct energy partitions and different effects on

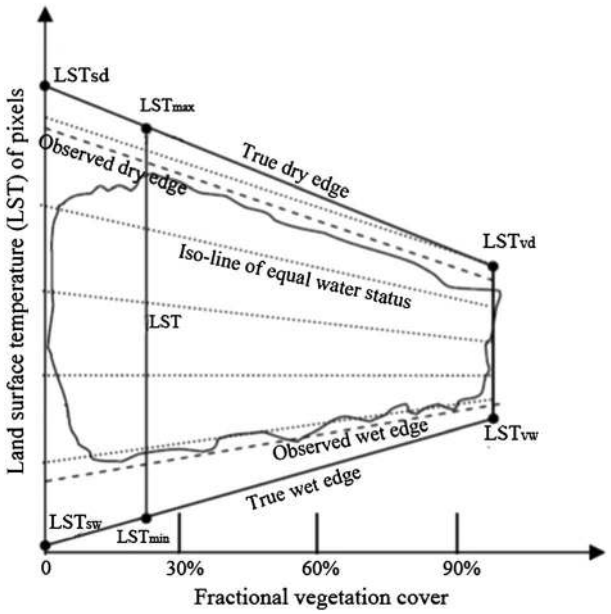

Figure 1. Scatterplot of surface temperature against vegetation fraction cover, where *v* and *s* denote vegetated area and bare ground, respectively, and *d* and *w* denote extremely dry and extremely wet water statuses, respectively. LST is the observed land surface temperature of a pixel. Its isoline of equal vegetation coverage interacts with the wet edge and dry edge at LST_{min} and LST_{max}, respectively.

surface temperature. Regulation of the land structure, e.g., by increasing green space coverage in an urban core, was suggested as the key in mitigating UHI intensity and adapting to climate change in cities [*Stone*, 2009; *Goldbach and Kuttler*, 2013]. Developing an effective UHI regulation requires a profound understanding of the energy partition processes and thermal regulation effects of various urban land types [*Oke*, 1982; *Grimmond et al.*, 2002] as well as quantification of the spatial pattern of energy balance [*Arnfield*, 2003], which was found to have unexpectedly high spatial heterogeneity even over apparently "homogeneous" developed areas [*Schmid et al.*, 1991; *Xu et al.*, 2008]. However, most earlier UHI studies either focused on in situ energy flux measures that represented only a small local-scale area within the heterogeneous urban environment [*Suckling*, 1980; *Spronken-Smith et al.*, 2000; *Grimmond*, 2005; *Cui et al.*, 2012] or were limited to describing the spatial patterns of surface temperature or sensible heat without the necessary information of LE and β for in-depth analysis of the mechanisms of energy partition underlying the thermal regulation functions of different urban land types [*Voogt and Grimmond*, 2000; *Xu et al.*, 2008; *Jenerette et al.*, 2011; *Mallick et al.*, 2013]. Spatially explicit studies that quantified the magnitudes of energy fluxes (R_n, LE, *H*) and the pattern of energy partition (i.e., β) at metropolitan scale were still rare [*Grimmond*, 2005].

The metropolitan area of Beijing is a focus of concern with regard to China's urbanization and environmental challenge. The city is facing severe environmental issues such as extreme heat and air pollution, which are related to impervious surface expansion [*Xiao et al.*, 2007; *Kuang*, 2012a]. *K. Wang et al.* [2007] found the albedo of urban land was lower than that of the rural area by 0.03–0.08, and the surface temperature of the city core could be 10°C higher than that of the surrounding rural areas in summer. *Yu et al.* [2013] found that the city's decadal mean land surface temperature has been steadily increasing since 1984. *Xiao et al.* [2007]'s study indicated that the mean land surface temperature rose by an average of 9.18°C as the natural land was replaced with impervious surfaces. *C. L. Zhang et al.* [2009] suggested that urban expansion would lead to reduced LE, increased β, and surface temperature, greater *H*, and reduced rainfall in Beijing. They further proposed to plant trees to mitigate the effect of UHI in Beijing. It is important to make such environmental projects cost effective, because the city has very high population density and land value. To achieve this goal, the thermal regulation functions of various urban LULC types should be quantified, and the spatial pattern of the major energy fluxes such as R_n, *H*, LE, and β should be mapped.

Although techniques have been well developed to retrieve land surface temperature (LST) from thermal infrared remote sensing images [*Li et al.*, 2013], we still need to find and improve a suitable methodology to map the spatial pattern of energy fluxes in urban landscapes. Quantitative models, such as the Surface Energy Balance Algorithm for Land model [*Bastiaanssen et al.*, 1998] and the Surface Energy Balance System model [*Su*, 2002] have been developed for surface energy partition at landscape scale [*Su et al.*, 2005; *Li et al.*, 2010]. These big-leaf models, however, are more suitable for areas with high-vegetation coverage than for heterogeneous landscapes like dry land or urban areas [*Verhoef et al.*, 1997]. With this limitation in mind, *Norman et al.* [1995] established a two-layer model of turbulent exchange to partition net radiation in sparsely vegetated areas. The application of this model, however, is limited because it relies on multiangle satellite data to provide directional measurements from two substantially different view angles. *Zhang* [2005] improved the two-layer model and

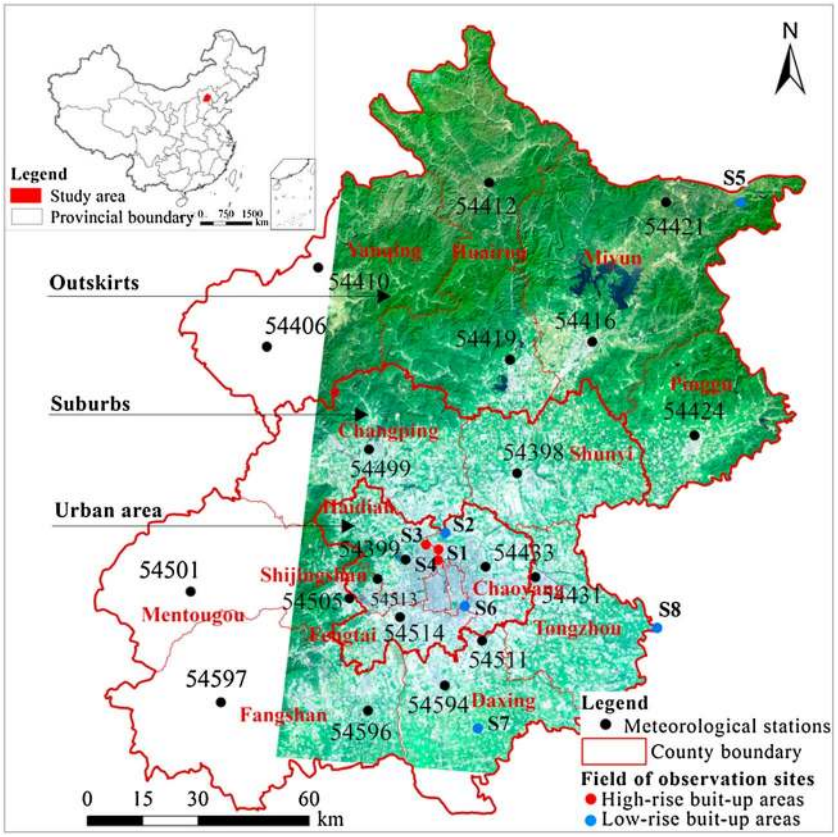

Figure 2. Location of the study area overlaid with the eddy covariance (EC) measurement sites and meteorological stations sites (Table 2) distributed on the false color (bands 4, 3, and 2) image of Landsat TM on 22 September 2009.

developed a more convenient Pixel Component Arranging and Comparing Algorithm (PCACA) model that requires only single-angle data on the basis of a triangle method and a Bowen ratio energy balance method to partition surface temperature and R_n of mixed pixels and finally estimate LE and H. Like the trapezoid method, PCACA utilizes the scatterplots of surface temperature and vegetation fraction cover (VFC), known as LST-VFC space, to determine the soil water status [*Carlson et al.*, 1995]. The method was based on the observations that surface temperatures of mixed pixels all fell into a trapezium constructed by vegetation coverage and surface temperature, in which the isolines of equal water status are nearly straight [*Carlson*, 2007] (Figure 1).

In Figure 1, the "true wet edge" of the trapezoid is related to surface conditions of potential evapotranspiration or maximum LE, while the "true dry edge" represents zero evapotranspiration or minimum LE. If the positions of the two edges are determined, the shape and structure of the trapezoid can be fixed and the consequent calculations of the surface heat fluxes could be done. In urban settings, LST_{sd} and LST_{sw} represent the points of true dry impervious surface and true water surface, respectively. LST_{vd} and LST_{vw} represent closed-canopy green spaces with true dry and water-saturated soils, respectively. According to *Zhang* [2005], the linear interpolation between wet and dry edges of the trapezium could be used to quantitatively estimate the water status or Bowen ratio of a pixel (equation (2)):

$$\beta \approx \left[\frac{\mathrm{LST} - \mathrm{LST}_{\min}}{\mathrm{LST}_{\max} - \mathrm{LST}}\right]_{\mathrm{VFC}} \tag{2}$$

where LST is the observed land surface temperature of the pixel. Its isoline of equal vegetation coverage interacts with the wet edge and dry edge at LST_{min} and LST_{max}, respectively. Earlier studies, however, were unable to accurately quantify the true wet/dry edges. Because these studies relied completely on remote sensing data and there were always an insufficient number of pixels to cover all kinds of soil wetness and vegetation fraction cover within their study areas, they had difficulty in determining true wet/dry edges. As an approximation, observed wet/dry edges (dashed lines in Figure 1) are often defined according to the

Table 1. Descriptions of Ground Observation Sites

ID	Site	Land Type	Latitude/Longitude	NDVI[a]	Land Surface Temperature (°C)[a]	Vegetation Coverage[b]	Latent Heat Ratio[b]
S1	Kexue Nanli	High-rise built-up area	116.3764°/39.9962°	0.12	31.00	0.2	0.302
S2	Olympic Forest Park	Urban park	116.4002°/40.0288°	0.45	24.38	0.75	0.664
S3	Ecological Research Center	High-rise built-up area	116.3428°/40.0092°	0.16	26.32	0.25	Not available
S4	Institute of Atmospheric Physics	High-rise built-up area	116.3709°/39.9744°	0.34	23.83	0.55	Not available
S5	Miyun	Woodland	117.3233°/40.6308°	0.35	20.35	0.65	0.732
S6	Botanical Teaching Garden	Urban park	116.4302° /39.8738°	0.51	22.44	0.75	Not available
S7	Daxing	Cultivated land	116.4271°/39.6213°	0.4	25.54	0.7	0.527
S8	Xianghe	Cropland and rural residence area	116.9500°/39.7830°	0.5	25.00	0.8	0.554

[a]Information retrieved from Landsat TM5 images.
[b]Field observations.

envelope shape of the actual scatterplot to represent the two actual extreme soil moisture conditions. Such approximation would introduce unknown errors. Furthermore, it is difficult to define the observed wet/dry edge (especially the wet edge) in practice because of the existence of outlying points that represent anomalous surfaces mainly due to cloud contamination [*Carlson*, 2007]. These outlying points need to be identified empirically and discarded from analysis. Due to subjective judgment, the previously used method to determine the trapezoid boundary often led to uncertainties. Furthermore, previous studies found that the albedo, R_n, momentum, heat flux, and moisture dynamics of the complex urban land surface differed significantly from those in rural areas [*Oke*, 1982; *Niemelä et al.*, 2001a, 2001b; *K. Wang et al.*, 2007]. *Offerle et al.* [2003] suggested that for an urban energy balance study, parameters of the remote sensing models designed for rural areas should be adjusted based on in situ measurements from urban sites.

In this study, the spatial patterns of energy fluxes in the Beijing metropolitan areas were retrieved from the Landsat TM thermal infrared images using the PCACA energy partition model. Synchronously measured in situ energy fluxes including *H* and LE from eight sites with different vegetation coverage were used to calibrate the model and define the true wet/dry edges. The observed downwelling/upwelling, longwave/shortwave radiations in these sites were used to validate the remote sensing results. Then the energy balance and thermal regulation functions of different urban LULC types were analyzed. The impacts of urban impervious surface and green space on heat reduction were quantified, and the spatial pattern of Bowen ratio was analyzed.

2. Materials and Methods

2.1. Study Area

The metropolitan area of Beijing is located in the northern region of the North China Plain (39°38′–40°51′N, 115°25′–117°30′E), with mountains in the west and northwest accounting for 62% of the total area; plains dominate the rest of the area (Figure 2). Beijing has a temperate continental monsoon climate with hot and rainy summers, cold and dry winters, a record minimum air temperature of −27.4°C, a record maximum air temperature of 42.6°C, and an average annual air temperature of 11°C (http://en.wikipedia.org/wiki/Beijing). The differences of minimum, maximum, and mean temperature between urban and suburban areas had an increasing trend influenced by urban heat island [*Xie and Cao*, 1996; *Wang and Hu*, 2006; *Zhan et al.*, 2013]. By the end of 2013, 21.51 million people lived in the city, and the population density was 1300 persons km^{-2} [*Beijing Municipal Bureau Statistics*, 2014]. Its total area is 16,801 km^2, with 1582.24 km^2 impervious surface area covering 72.6% of the built-up area [*Kuang*, 2011; *Kuang*, 2012a; *Kuang et al.*, 2013]. Beijing has experienced fast urban expansion in the past three decades, with more than a threefold increase in built-up area since 1984 [*Kuang*, 2012b]. Accompanied by the rapid urbanization, severe urban environmental issues such as extreme heat and air pollution have emerged [*Xiao et al.*, 2007; *Ke et al.*, 2014]. To improve the city's environment, large-scale urban greenery projects have been installed in recent years, most notably the Olympic Forest Park, an artificial green space that covers 11.59 km^2 of the city land. An outskirt city greenbelt also has been formed. The total green space in the urban area is now approximately 304.6 km^2, and the greenbelt is approximately 1097 km^2 in outskirt [*Beijing Municipal Institute of City Planning and Design*, 2004].

Table 2. Observed Air Temperature in 20 Meteorological Stations on 22 September 2009

Site ID	Latitude/Longitude (deg)	Elevation (m)	Air Temperature (°C)
54596	116.1333/39.6833	39.2	20.91
54594	116.3500/39.7167	37.6	20.94
54597	115.7333/39.7333	407.7	23.34
54511	116.4667/39.8000	31.3	20.25
54514	116.2500/39.8667	55.2	21.51
54431	116.6333/39.9167	43.3	19.68
54505	116.1167/39.9167	92.7	21.30
54433	116.5000/39.9500	35.3	19.70
54513	116.2000/39.9500	65.6	21.27
54501	115.6833/39.9667	440.3	21.25
54399	116.2833/39.9833	45.8	20.42
54398	116.6167/40.1333	28.6	19.81
54424	117.1167/40.1667	32.1	21.00
54499	116.2167/40.2167	76.2	20.725
54419	116.633340.3667	75.7	20.00
54416	116.8667/40.3833	71.8	19.68
54406	115.9667/40.4500	487.9	17.28
54410	116.1333/40.6000	1224.7	15.37
54421	117.1167/40.6500	293.3	21.25
54412	116.633340.7333	331.6	18.61

2.2. Remote Sensing Data and Eddy Flux Measurements

LST and energy fluxes of the study area at 10:43 A.M. on 8 September 2004, 22 September 2009, and 4 September 2014 were retrieved from the Landsat TM images with 30 m spatial resolution at multispectral band and 120 m resolution at the thermal infrared radiation band (10.45–12.5 μm). The TERRA/MODIS remote sensing images (MOD021KM and MOD03 data) of the same time were used to estimate atmospheric transmittance. Following *Zhang et al.* [2008], ground-synchronized measurements of surface temperature at the center of Miyun Reservoir, the largest lake in Beijing and at the center of an airfield runway (at least 80 m from the closest green space) were conducted to estimate the LST_{sw} and LST_{sd}, respectively (Figure 2). Eddy flux measurements of downwelling/upwelling longwave/shortwave radiations from eight sites were collected (Table 1). Three of the eight sites (S1, S3, and S4) located in the high-rise built-up areas in the inner city (Figure 2; for a photo of the eddy flux tower, see Figure S1 in the supporting information). Other sites located in the parks and rural areas with a more open landscape. These observations were used to validate the remote sensing-retrieved radiation fluxes [*Jia et al.*, 2012; *Liu et al.*, 2013; *Miao et al.*, 2012]. Five of the eight sites also recorded LE and *H* from which the latent heat ratio (see equation (10)) were calculated (Table 1). These latent heat ratio observations, together with the estimated vegetation coverage and the remote sensing-retrieved LST of the sites were used to derive the slopes of the true wet/dry lines (see section 2.3.3).

Ground-synchronized measurements of air temperatures (at 2 m) from 20 meteorological stations were analyzed to develop the air temperature map for Beijing (Table 2 and Figure 2) (http://cdc.cma.gov.cn/home.do). First, the temperature lapse rate was estimated with a linear regression between the elevations and the temperature records of the stations. Then the reference temperature (elevation = 0) was calculated based on the lapse rate for each station. Next, the reference temperature map of Beijing was developed from the reference temperature of the meteorology stations with the inverse distance-weighted interpolation. Finally, with the lapse rate and the 120 m resolution digital elevation model of the city, the near-surface temperature map of Beijing was developed from the reference temperature map. A flow chart illustration of the methodology is provided in Figure 3.

2.3. Retrieving Energy Fluxes of Beijing From Remote Sensing Data

To develop the LE and *H* maps of Beijing, we first estimated vegetation coverage based on the Landsat TM data. Then, the LST map of Beijing was retrieved from the Landsat TM thermal infrared band using the monowindow algorithm developed by *Qin et al.* [2001]. Finally, the PCACA energy partition model, which was calibrated with synchronously measured in situ eddy covariance fluxes, was used to partition the surface available energy, i.e., $R_n - G$ (see supporting information for retrieval of the radiation fluxes) into LE and *H* and derive the Bowen ratio map of Beijing.

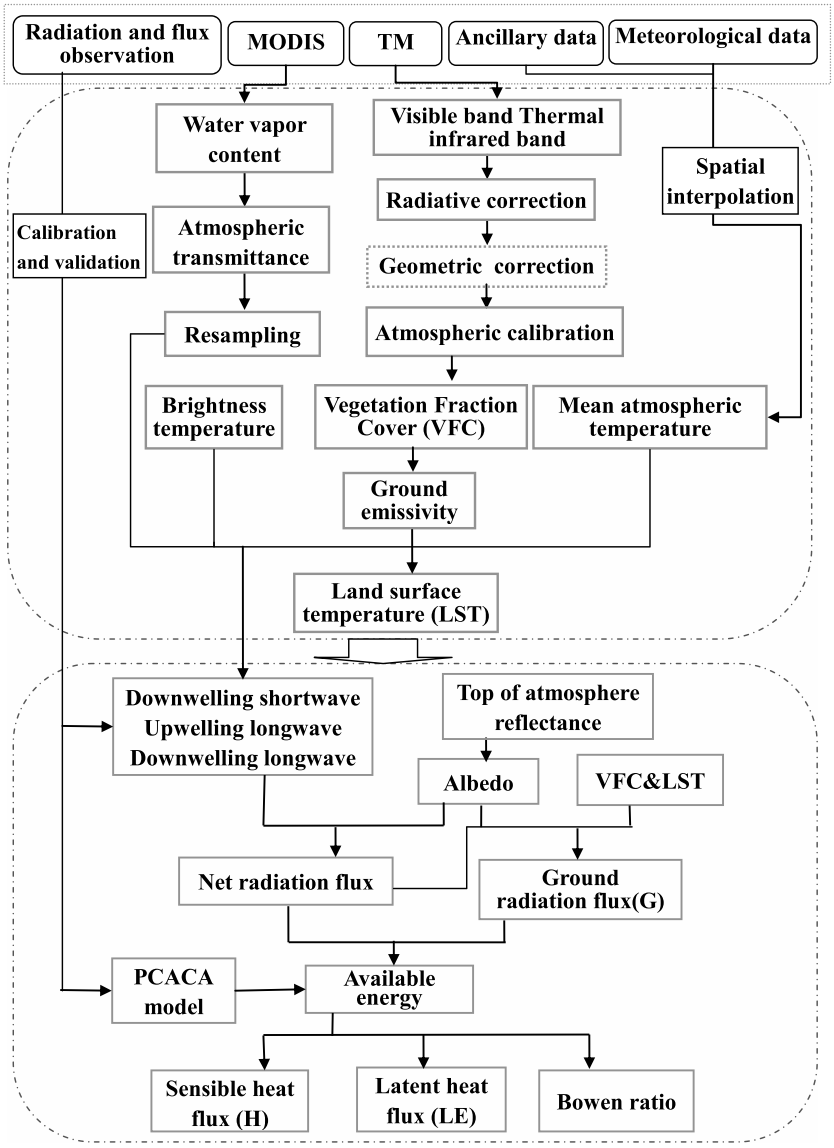

Figure 3. A flow chart illustration of the research methodology.

2.3.1. Vegetation Coverage Retrieval

This study calculated the VFC with the simple and widely used dimidiate pixel model [*Leprieur et al.*, 2000; *Jiang et al.*, 2006], which estimates the VFC as a function of the atmospherically corrected normalized difference vegetation index (NDVI) values [*Goetz*, 1997]:

$$\mathrm{VFC} = (\mathrm{NDVI} - \mathrm{NDVI}_0)/(\mathrm{NDVI}_V - \mathrm{NDVI}_0) \tag{3}$$

Let $Y = \mathrm{NDVI} - \mathrm{NDVI}_0$, and $k = \mathrm{NDVI}_v - \mathrm{NDVI}_0$, we have

$$Y = k \times \mathrm{VFC} \tag{4}$$

where NDVI_0 and NDVI_v are NDVI values of bare ground and fully vegetated area, respectively. Depending on the location and time of observation, NDVI_0 and NDVI_v could have various values [*Carlson and Ripley*, 1997; *Gutman and Ignatov*, 1998; *Leprieur et al.*, 2000]. NDVI_0 was set to 0.04, which is the mean NDVI of the Beijing airport runway according to the Landsat TM 5 data. To estimate NDVI_v, equation (3) was fitted to the observed VFCs and their corresponding Y values ($= \mathrm{NDVI} - \mathrm{NDVI}_0$) in eight sites (Table 1). The fitting is statistically significant at 95% with adj-$R^2 = 0.95$. Because the fitted $k = \mathrm{NDVI}_v - \mathrm{NDVI}_0 = 0.547$, $\mathrm{NDVI}_v \approx 0.59$. Finally, the VFC map of Beijing was calculated using equation (3) based on the Landsat TM NDVI data.

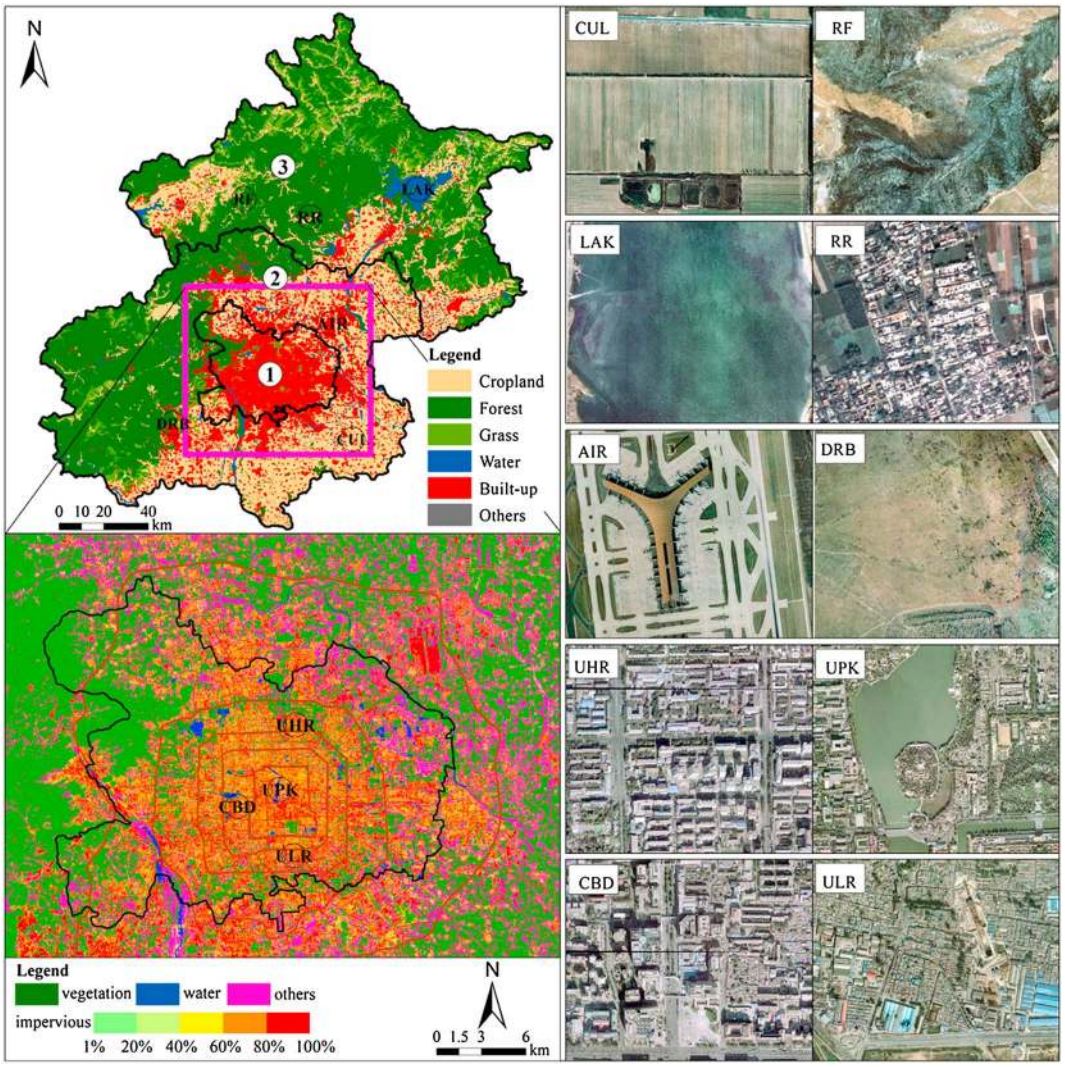

Figure 4. Land use map of Beijing retrieved from Landsat TM image [*Kuang*, 2012a] and the selected sites representing 10 land use types. Urban park (UPK), central business district (CBD), urban high-rise residential areas (UHR), urban low-rise residential areas (ULR), airport (AIR), rural forest (RF), lakes (LAK), rural residential areas (RR), cultivated land (CUL), and dry riverbed (DRB). The top left shows the boundaries of (1) urban area, (2) suburbs, and (3) outskirts of Beijing. The pink line outlines a sample area at the central Beijing, whose pixels were scatterplotted in Figure 5.

2.3.2. Land Surface Temperature Retrieval

The LST of Beijing was retrieved from the thermal infrared radiation band (band 6) of Landsat TM5 using the monowindow algorithm developed by *Qin et al.* [2001]:

$$\begin{aligned} \mathrm{LST} &= [-67.355351\times(1-C-D)+(0.458606\times(1-C-D)+C+D)\times T_6 - D\times T_a]/C \\ C &= \varepsilon\times\tau \\ D &= (1-\tau)\times[1+(1-\varepsilon)\times\tau] \end{aligned} \tag{5}$$

where ε is ground emissivity, τ is atmospheric transmittance (see the supporting information for methods to derive ε and τ), T_6 is the at-sensor brightness temperature, and T_a represents the effective mean atmospheric temperature. According to *Qin et al.* [2001] and *Sobrino et al.* [2004], T_a was estimated as

$$T_a = 16.0110 + 0.92621\times(\mathrm{T}+273.15) \tag{6}$$

and T_6 was estimated according to *Markham and Barker* [1987] and the Handbook of Landsat 7 (landsathandbook.gsfc.nasa.gov; last visited on 15 Oct 2014):

$$T_6 = 1260.56/\ln\left(1+60.776/L_{(\lambda)}\right) \tag{7}$$

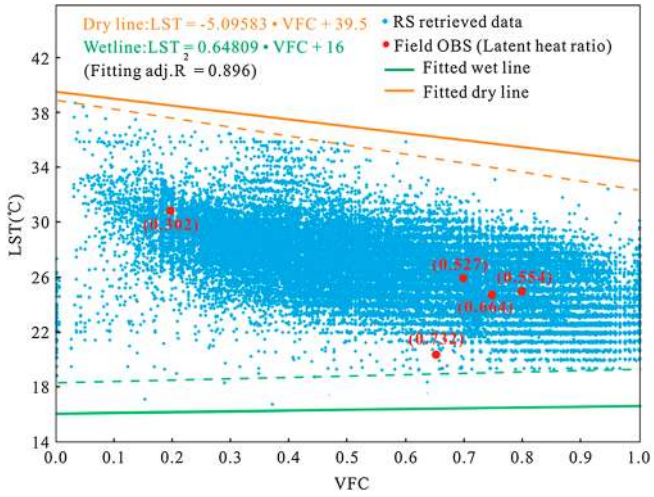

Figure 5. The wet edge (green) and dry edge (brown) derived in this study by fitting the in situ measurements of latent heat ratios from five sites (red dots) to the PCACA model (equation (11)). Observed latent heat ratios of the five sites are listed in the parentheses in red. LST-VFC scatterplots of 264,845 samples from central Beijing were enclosed by the trapezium bounded by the wet and dry edges. Dotted lines indicate the observed edges based on the plots of 264,845 samples.

with $L_{(\lambda)} = 0.005632156 \times Q_{dn} + 0.1238$, where Q_{dn} is the grey level for the analyzed pixel of the TM image. T (°C) is the near-surface air temperature (see section 2.2). More details about this algorithm and its sensitivity can be found in the work of *Qin et al.* [2001].

2.3.3. Latent Heat and Sensible Heat Partition

As introduced above, equation (2) can be used to estimate the Bowen ratio of any pixel in the study region. The major challenge is to identify the true wet edge and dry edge in the study region for the PCACA trapezoid method so that the values of LST_{min} and LST_{max} can be calculated (Figure 1). Following *Zhang et al.* [2008], LST_{sw} and LST_{sd} were estimated with ground-synchronized measurements of surface temperatures in water bodies and at an airfield runway in the study area, respectively. Then LST_{max} and LST_{min} in Figure 1 can be represented by

$$\left.\begin{aligned} LST_{max} &= k_{dry} \times VFC + LST_{sd} \\ LST_{min} &= k_{wet} \times VFC + LST_{sw} \end{aligned}\right\} \quad (8)$$

where k_{dry} and k_{wet} are slopes of the dry/wet edges. By substituting LST_{max} and LST_{min} in equation (2) with equation (8), we have

$$\beta \approx \frac{-k_{wet} \times VFC - (LST_{sw} + LST)}{k_{dry} \times VFC + (LST_{sd} - LST)} \quad (9)$$

According to equation (1), we can define latent heat ratio (L_r) as $L_r = \frac{LE}{R_n - G} = \frac{LE}{LE+H} = \frac{1}{1+\beta}$. Then based on equation (9), we have

$$L_r = \frac{1}{1+\beta} \approx \frac{k_{dry} \times VFC + (LST_{sd} - LST)}{(k_{dry} - k_{wet}) \times VFC + (LST_{sd} - LST_{sw})} \quad (10)$$

$$LST = k_{dry} \times VFC + (k_{wet} - k_{dry}) \times VFC \times L_r - (LST_{sd} - LST_{sw}) \times L_r + LST_{sd} \quad (11)$$

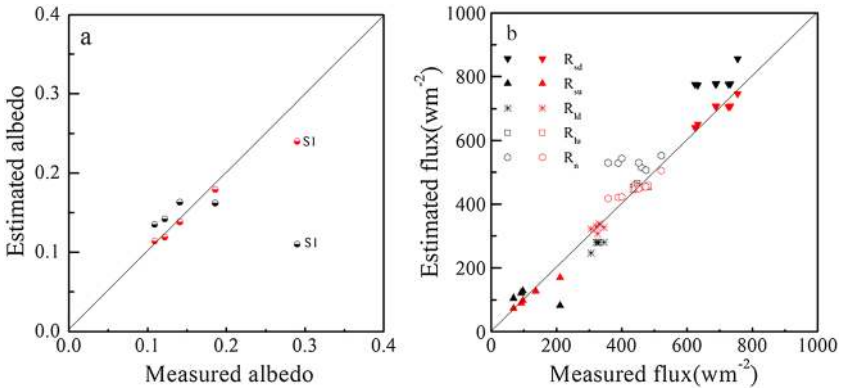

Figure 6. The validation of remote sensing-retrieved radiation fluxes using in situ observed (a) albedo and (b) heat fluxes. R_{sd}: downwelling shortwave radiation; R_{su}: upwelling shortwave radiation; R_{ld}: downwelling longwave radiation; R_{lu}: upwelling longwave radiation; R_n: net radiation flux.

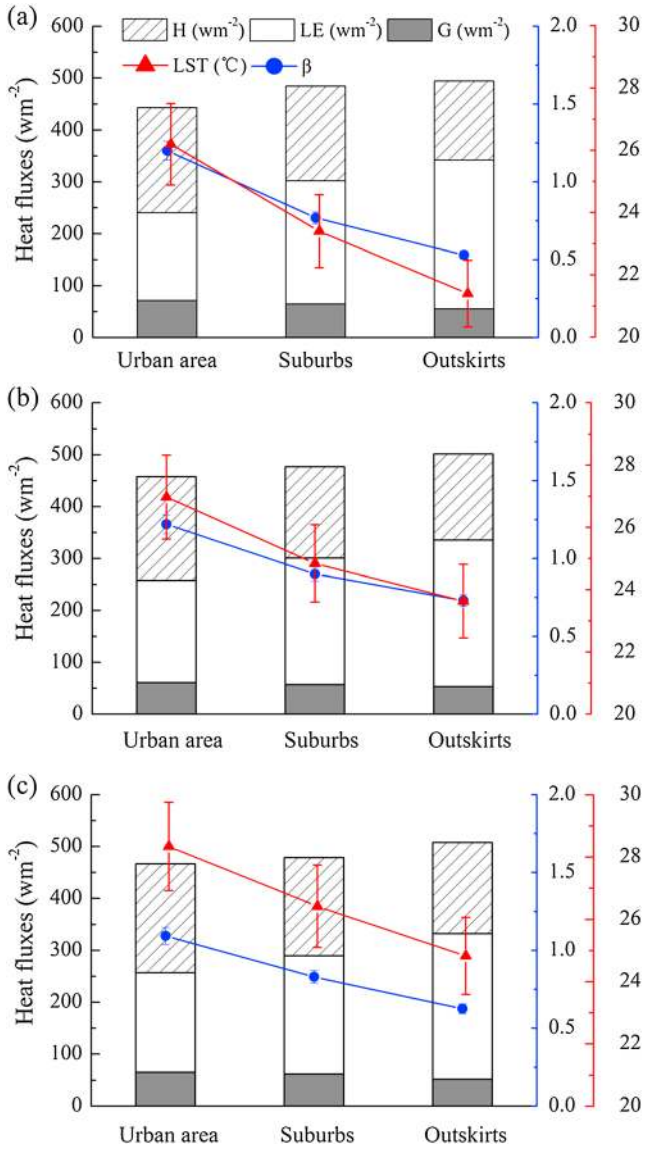

Figure 7. A comparison of the flux, LST, and net radiation data across urban area, suburbs, and outskirts (black axis: heat flux; blue axis: Bowen ratio; red axis: LST) in (a) 2004, (b) 2009, and (c) 2014.

Based on the VFC and LST retrieved from Landsat TM images and the synchronously measured L_r from five sites in Beijing (Table 1), a nonlinear regression was conducted to derive the value of k_{dry} and k_{wet}. Finally, with all the parameters (LST_{sd}, LST_{sw}, k_{dry}, and k_{wet}) quantified and the remote sensing-retrieved VFC and LST as inputs, equation (9) was used to calculate the Bowen ratio of each pixel in Beijing. Then the LE and H of Beijing were calculated from the surface available energy $R_n - G$ (see supporting information for retrieval of radiation fluxes).

2.3.4. Spatial Overlay Analysis

To analyze the spatial pattern of heat fluxes, we compared the changes in LST, R_n, H, LE, and β among the outskirts (impervious surface coverage $< 5\%$), suburbs, and urban area (impervious surface coverage $> 70\%$). We also analyzed the regulation effects of 10 LULC types on LST and heat fluxes. These land types are urban park (UPK), central business district (CBD), urban high-rise residential area (UHR), urban low-rise residential area (ULR), airport (AIR), rural forest (RF), lake (LAK), rural residential area (RR), cultivated land (CUL), and dry riverbed (DRB) (Figure 4).

3. Results and Analysis

3.1. Model Calibration and Validation With Field Measurements

The mean value of 80 synchronously measured water surface temperatures indicates the true water surface temperature $LST_{sw} \approx 16.0 \pm 0.3$°C. The mean value of 80 LST measurements at an airfield runway in the study area indicates the true dry surface temperature $LST_{sd} \approx 39.5 \pm 0.8$°C. With the values of LST_{sw} and LST_{sd} known, the VFC, LST, and L_r (see equation (11)) measured in five sites (Table 1) were fitted to equation (11) to estimate/calibrate the values of k_{dry} and k_{wet}. The fitting was statistically significant at 95% with adj-$R^2 = 0.896$. The result showed $k_{dry} = -5.09583$ and $k_{wet} = 0.64809$. With these parameter values, the values of LST_{vd} and LST_{vw} in the PCACA trapezium (Figure 1) can be calculated with equation (8):

$$\left.\begin{aligned} LST_{vd} &= k_{dry} \times 100\% + LST_{sd} = 34.40°C \\ LST_{vw} &= k_{wet} \times 100\% + LST_{sd} = 16.65°C \end{aligned}\right\} \quad (12)$$

Further, the Bowen ratio of each pixel can be estimated from VFC and LST using the formula

$$\beta \approx \left[\frac{LST - 0.64809 \times VFC - 16}{-LST - 5.09583 \times VFC + 39.5}\right]_{VFC} \quad (13)$$

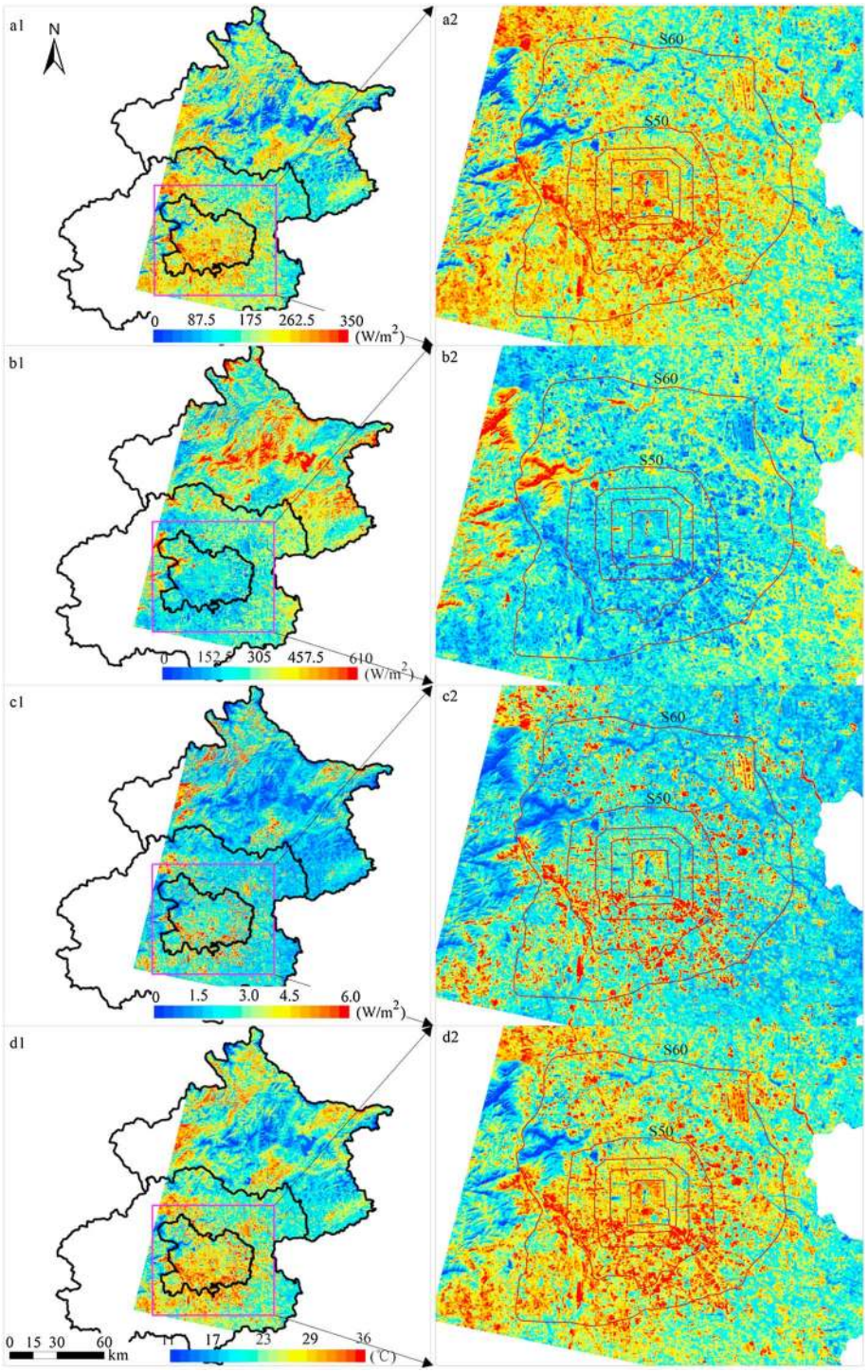

Figure 8. The spatial distribution of (a) sensible heat, (b) latent heat, (c) Bowen ratio, and (d) land surface temperature in Beijing on 22 September 2009.

For visual evaluation, 264,845 pixel values from a 64.75 km by 58.90 km sampling area at central Beijing (Figure 4) were plotted onto the LST-VFC space (Figure 5).

The Landsat TM5-retrieved shortwave solar radiation, upwelling shortwave radiation, downwelling longwave radiation, upwelling longwave radiation, and R_n were validated against the in situ measurements from eight sites listed in Table 1. The remote sensing-retrieved heat fluxes and albedo were consistent with the field

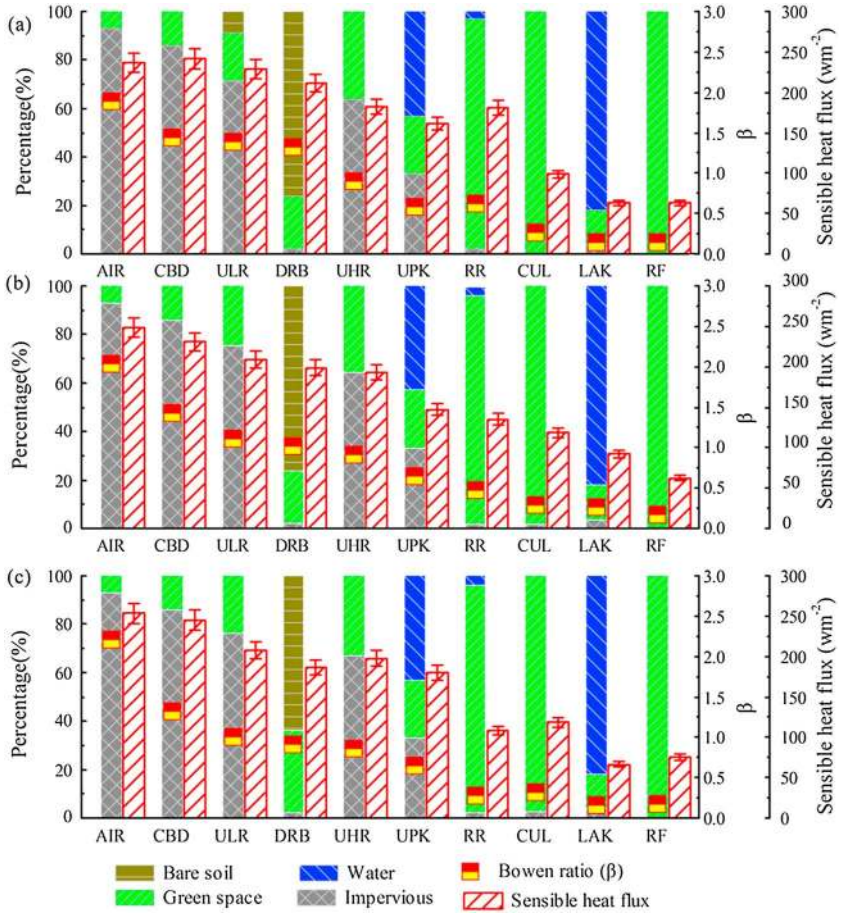

Figure 9. Land composition, and sensible heat fluxes and Bowen ratios of 10 land use types based on sample analysis for the year (a) 2004, (b) 2009, and (c) 2014, including samples from urban park (UPK), central business district (CBD), urban high-rise residential areas (UHR), urban low-rise residential areas (ULR), airport (AIR), rural forest (RF), lakes (LAK), rural residential areas (RR), cultivated land (CUL), and dry riverbed (DRB).

measurements (Figure 6). The root-mean-square errors (RMSEs) of the surface downwelling and upwelling shortwave radiation data were 20.02 W/m^2 and 10.20 W/m^2, respectively. The RMSEs of the downwelling and upwelling longwave surface radiation data were 12.68 W/m^2 and 6.47 W/m^2, respectively, and the RMSE of R_n was 20.72 W/m^2.

3.2. Spatial Pattern of Land Surface Temperatures and Heat Fluxes in the Metropolitan Area of Beijing

We found consistent spatial pattern of LST and heat fluxes in 2004, 2009, and 2014. At regional scale, the surface temperature increased from 21.40–24.83°C (based on the LST in 2004, 2009, and 2014) in the outskirts to 23.37–26.42°C in suburbs to 26.19–28.34°C in the urban area, indicating a mild urban heat island in Beijing (Figure 7). The mean Bowen ratio increased significantly from 0.53–0.62 in the outskirts to 0.77–0.90 in suburbs to 1.09–1.22 in urban area, mainly due to the significant differences in LE, which declined from 281–287 W/m^2 in the outskirts to 228–244 W/m^2 in suburbs to 169–197 W/m^2 in the urban area. However, the soil heat flux increased from 61–72 W/m^2 in the urban area to 57–65 W/m^2 in suburbs to 52–55 W/m^2 in the outskirts.

Figure 8 shows the strong spatial heterogeneities of LST and heat fluxes in 2009. Similar patterns were found in 2004 and 2014. Even in the urban area, water bodies had very low surface temperatures and low Bowen ratios in contrast to the heat flux signatures of the nearby built-up areas. We found a large area with low LST and Bowen ratio in the midnorth of the outskirts region. This area contains closed-canopy forests located west of the largest water body, Miyun Reservoir, in Beijing. The high LE of these forests, especially those located close to Miyun Reservoir, indicated that they had good soil water supply. Their mean LST was about 17.11°C, close to the LST_{vw} (= 16.65°C) that represents closed-canopy green spaces with true water-saturated

soils (equation (12) and Figure 1). In the urban area, the northern part has a lower mean Bowen ratio ($\beta = 1.02$) compared to the southern part ($\beta = 1.9$), possibly due to the higher proportion of recently developed green spaces in the northern Beijing [*Kuang*, 2012b]. This difference could also be related to the different land use compositions. While the southern part of the urban area was mainly covered by traditional low-rise residential land use, the northern part was mainly covered by modern high-rise residential/commercial land uses. Therefore, we further analyzed the characteristics of heat fluxes among different land use types.

3.3. Characteristic Heat Fluxes of Different Land Use Types

Samples of 10 land use types—UPK, CBD, UHR, ULR, AIR, RF, LAK, RR, CUL, and DRB—were analyzed (Figure 4). AIR had the highest Bowen ratio of 1.90–2.20, while the LAK and RF had the lowest Bowen ratio of 0.15–0.26 (Figure 9). As a result, the sensible heat of AIR was about 4 times that of RF and LAK, while the latent heat of RF and LAK were about 4 times that of AIR. The Bowen ratios of urban land uses were generally higher than those of their rural counterparts. For example, the Bowen ratio of UPK was more than 3 times that of RF, and the mean Bowen ratios of UHR and ULR were more than twice the value of RR. These patterns were consistent from year to year (Figure 9).

4. Discussions

4.1. Improving Urban Heat Flux Partitioning With a New PCACA Model Calibration Method

Urban heat island effect is related to the spatial pattern of urban LST, which is the synthetic result of the heat and water balance in the surface. Well-developed remote sensing methodologies are available for retrieving R_n. How to excavate and extract the information of energy partition is a key problem. Analytical models such as the residence network two-layer model can estimate the LE and H. However, these models require a large number of parameters, such as surface roughness, local wind speed, atmospheric stability, friction velocity, Mourning-Obukhov length, and boundary layer height, which are difficult to quantify even at site scale [*Choudhury*, 1989]. Considering the complexity in spatial pattern and energy processes in urban landscapes, it is very important to find a practical model for urban heat balance research.

Moran et al. [1989] investigated the heat flux partitions in 18 fields with various VFCs and soil-water statuses and found that the LSTs for different VFCs all fell into a trapezium in the LST-VFC space. More importantly, they found that isolines of equal soil water availability were nearly straight in the trapezium, which indicate that the linear interpolation between wet and dry edges of the trapezium could be used to quantitatively estimate the soil water status and heat partition of alfalfa [*Zhang*, 2005]. The trapezoid method, as represented by the PCACA model [*Zhang*, 2005], avoids the necessity to quantify various surface resistance parameters that cannot be estimated by remote sensing and is more practical for urban study. However, previous PCACA studies were unable to quantify the true dry/wet edges of the trapezium because of the existence of outlying points that represent anomalous surfaces [*Carlson*, 2007]. They had to rely on empirical "observed dry/wet edges" as an approximation. This empirical approach to determine the trapezoid boundary often leads to uncertainties due to subjective judgments [*Zhang et al.*, 2008].

Our study modified the formula of the PCACA (equation (11)), making it possible to calibrate the model parameters with field observations. In our Beijing metropolitan case study, the LST-VFC trapezium was constructed by fitting the PCACA model to satellite-retrieved VFC and LST and five synchronously measured latent heat ratios, with high R^2 (= 0.896). With 264,845 samples from central Beijing, we illustrate that the "observed trapezium" developed with the empirical approach by previous studies could significantly differ from the true trapezium, especially for the definition of the dry edge. The traditional empirical approach requires a large number of pixels over an area with wide ranges of soil wetness and vegetation fraction cover, which usually cannot be satisfied within a limited study area [*Zhang et al.*, 2008]. Therefore, our model calibration method is more accurate and suitable for landscape studies such as urban heat flux partitioning.

4.2. Heat Regulating Effects of Different Urban Land Use Types

Our study revealed strong spatial heterogeneity in LST and highlighted the distinct heat fluxes among different land use types (Figure 9). For example, the Bowen ratio of the CBD was nearly 1.24 times higher than that of the urban park. Similarly, *Y. Liu et al.* [2012] found the Bowen ratio of commercial land was about 1.56 times higher than that of the public green space in the Saitama Prefecture city, Japan. Like our findings in the

urban airport, *Y. Liu et al.* [2012]'s study indicated that the Bowen ratio increased with higher artificial land covers (i.e., impervious surface). Our estimated urban park Bowen ratios (0.58–0.65), however, was much higher than that in the Saitama Prefecture city (0.31), possibly due to the dryer climate and lower vegetation coverage of Beijing [*Y. Liu et al.*, 2012]. According to an eddy flux measurement, the daytime Bowen ratio in Beijing's urban park was about 0.5 [*X. X. Wang et al.*, 2007], very close to our estimation. Like us, *Y. Liu et al.* [2012] found that the water bodies in urban had the lowest Bowen ratio. In contrast to the different estimates for urban park, our estimated Bowen ratio for urban water bodies (0.15–0.26) in Beijing was very close to the estimates in Saitama Prefecture city by *Y. Liu et al.* [2012], highlighting the stable heat flux characteristics of water bodies.

Even similar land use types can have different heat fluxes. The sensible heats of urban residential areas were significantly higher than those of the rural residential areas in Beijing. Furthermore, the sensible heat of the low-rise residential area was higher than that of the high-rise residential area in the urban area. This difference could partially explain why the southern part of the city (mainly covered by low-rise residential lands) had higher LST than the northern part (prevailed by high-rise residential lands), despite the strong sensible heat fluxes from the many CBDs in the northern city (Figure 8). The significant difference in sensible heat among various land use types raises the possibility of regulating UHI effect by changing the land use composition of an urban landscape, for example, by translocating the airport from the urban area of Beijing to the rural area. To reduce heat stress on city dwellers, a recommendation for the municipal administrator of Beijing might be to upgrade the traditional low-rise residential areas to modern high-rise residential areas that have lower sensible heat. As more and more families can afford automobiles, city dwellers will gradually be moving from urban residential areas to rural residential areas, where heat stress would be much weaker (Figure 9). Further, preserving urban lakes could effectively reduce sensible heat in the city, as shown by the strong contrast in sensible heat between the lakes and the surrounding CBDs in the center of Beijing (Figure 8a).

The differences in LST and sensible heat among various land use types were closely related to their distinct heat flux partitions or Bowen ratios. The lower the Bowen ratio, the more R_n was dissipated as latent heat through evapotranspiration; hence, less sensible heat remained. Figure 9a indicates that the Bowen ratio was positively correlated to the fraction of impervious surface plus bare soil and negatively correlated to the fraction of vegetation plus water. *Arnfield* [2003] suggested that the UHI effect is mainly caused by the enhanced energy retention of urban canyons, an urban structure manifested by streets cutting through dense blocks of high-rise manmade buildings. However, many previous observations suggested that the strong sensible heats from the urban impervious surfaces were the main reason of UHI, while green spaces could effectively cool down the temperature even in city centers [*Pu et al.*, 2006; *X. X. Wang et al.*, 2007; *Buyantuyev and Wu*, 2010; *Yan et al.*, 2010; *Y. Liu et al.*, 2012]. Our study indicated that the land surface composition could be a more important factor than the urban structure in determining the magnitude and structure of UHI at daytime. Although the northern part of Beijing had many more skyscrapers, and thus stronger urban canyon effects, than the southern part [*Xiao et al.*, 2008], we found lower sensible heat and LST in the north (Figure 8). That was probably because the recent large-scale urban greenery projects in the north, most notably Olympic Forest Park, increased the vegetation cover and energy dissipated through plant transpiration [*Sun et al.*, 2011]. Similarly, we found the high-rise residential area has lower sensible heat than the low-rise residential area (Figure 9), although the former, with a much lower sky view than the latter, should have a stronger urban canyon effect than the latter. The lower sensible heat in the high-rise residential area may be explained by its higher fraction of green space than the low-rise residential area as well as the cooling effects from its higher shaded areas (Figure 9). Our analysis showed that the fraction of shaded land surface in UHR was about 164% higher than in URL. According to our estimation, the cooling effects of the extra shadows in the UHR might contribute to ~5% for its lower LST than URL (see the supporting information for a description of the shadow effect analysis). Therefore, a larger portion of the observed temperature difference between UHR and ULR may be related to other mechanisms such as the green space cooling effect. Urban green spaces usually have strong evapotranspiration and are effective in dissipating energy through LE [*Imhoff et al.*, 2010]. In fact, thermal dissipation through plant's transpiration was an important ecological service provided by urban vegetation in China [*Jim and Chen*, 2009]. *Chen et al.* [1998] estimated that each 1 m^2 forest canopy could dissipate 507 $J\,d^{-1}$ and the 16,577 ha urban forest in Beijing could dissipate $30.7 \times 109\ kJ\,d^{-1}$.

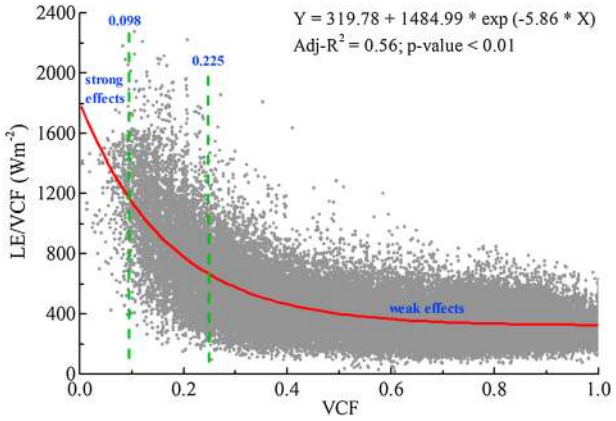

Figure 10. The nonlinear relationship between heat regulation strength of urban vegetation (W m^{-2} canopy area; calculated as LE/VFC) and vegetation coverage (VFC) based on the Landsat TM-retrieved VFC and heat fluxes in 2004, 2009, and 2014 in Beijing. The VFC thresholds, 0.098 and 0.225, are used to delineate the areas where vegetation have relatively strong (VFC < 0.098) and low (VFC > 0.225) thermal regulation strength (please find the detailed discussion at the end of section 4.2).

Like others [*Chen*, 2006; *Zhang et al.*, 2006], *Chen et al.* [1998] assumed heat regulating strength of forest canopy, i.e., latent heat per canopy area, unchanged from place to place or a linear positive correlation between LE and VFC. Other studies also assumed linear positive correlation between urban impervious surface coverage and LST [*Yuan and Bauer*, 2007; *Xiao et al.*, 2007; *Zhang et al.*, 2010]. Our study, however, found that the thermal dissipating strength of forest canopy, calculated as LE/VFC, declined exponentially with increased VFC; in other words, the lower the vegetation coverage, the higher the LE intensity in unit canopy area (Figure 10). Supported by microscale advection from contiguous dry impervious surface, green spaces in intensively built-up areas were found to exhibit very high latent heat, even in excess of net solar radiation [*Oke*, 1979]. As a result, small patches of urban green spaces in the matrix of impervious surface could act as net heat sinks (i.e., a downward directed *H*) [*Spronken-Smith et al.*, 2000].

An exponential fitting (p value < 0.01; adj-$R^2 = 0.56$) in Figure 10 show that

$$\mathrm{LE/VFC} = 319.78 + 1484.99 \times e^{-5.86 \times \mathrm{VFC}} \tag{14}$$

Based on the remote sensing-retrieved LE and VFC data in 2004, 2009, and 2014, the mean thermal dissipating strength of vegetation canopy in Beijing ($\mathrm{LE_{mean}/VFC_{mean}}$) was 437 W m^{-2}, which translates into a VFC = 0.225 according to equation (14). Therefore, if the VFC of an urban area > 0.225, the thermal dissipating strength of its vegetation canopy was likely lower than the mean thermal dissipating strength of vegetation in Beijing. Expanding green spaces in these areas will have relatively low heat regulating effect. In intensively built-up areas whose VFC < 0.098, the thermal dissipating strength of vegetation could be more than twice larger than the mean thermal dissipating strength (i.e., 437 W m^{-2}) (Figure 10). Expanding green spaces in these areas will be very effective in alleviating local heat stress. Based on the above analysis, Figure 11 shows the areas where urban greenery project could be very effective, effective, and less effective in heat stress regulating. We found that urban greening will be "very (twice) effective" in heat regulating in about 1.1% of the Beijing metropolitan area. According to the study, we recommend the municipal administrator to focus on expanding the green spaces in the city center and the southern part of built-up area.

4.3. Uncertainties in the Estimated Longwave Radiation Emission

It should be noted that we did not consider the radiometric anisotropy in urban, which could negatively affect the accuracy of the estimated surface longwave radiation emission and LST [*Voogt and Oke*, 1998; *Suleiman and Crago*, 2002]. The global (or hemispherical) longwave radiation (R_{lu}) of an urban canopy consists of the emission/reflection from building walls ($R_{lu,wall}$) as well as the emission from urban floor and roof ($R_{lu,floor}$). The relative contribution of $R_{lu,wall}$ and $R_{lu,floor}$ depends on the roof coverage and the sky view factor of the urban canyon [*Johnson and Watson*, 1984]. Using the nadir-view thermal infrared image of the TM Landsat, we were only able to estimate the longwave emission from the floors and roofs, as the walls were "invisible" to the nadir sensor. Because the global longwave radiation was calculated based on the retrieved $R_{lu,floor}$, our approach implicitly assumed the intensity of $R_{lu,wall} = R_{lu,floor}$. However, due to the different incident solar radiations, the surface temperatures and longwave emissions of the floors and roofs are higher than that of the walls in most time of a year [*Sugawara and Takamura*, 2006]. Therefore, we might have overestimated the mean LST and global R_{lu} of urban areas in Beijing, particularly in the high-rise built-up areas where the sky view factor was small and $R_{lu,floor}$ was a key component of the global R_{lu} [*Soux et al.*,

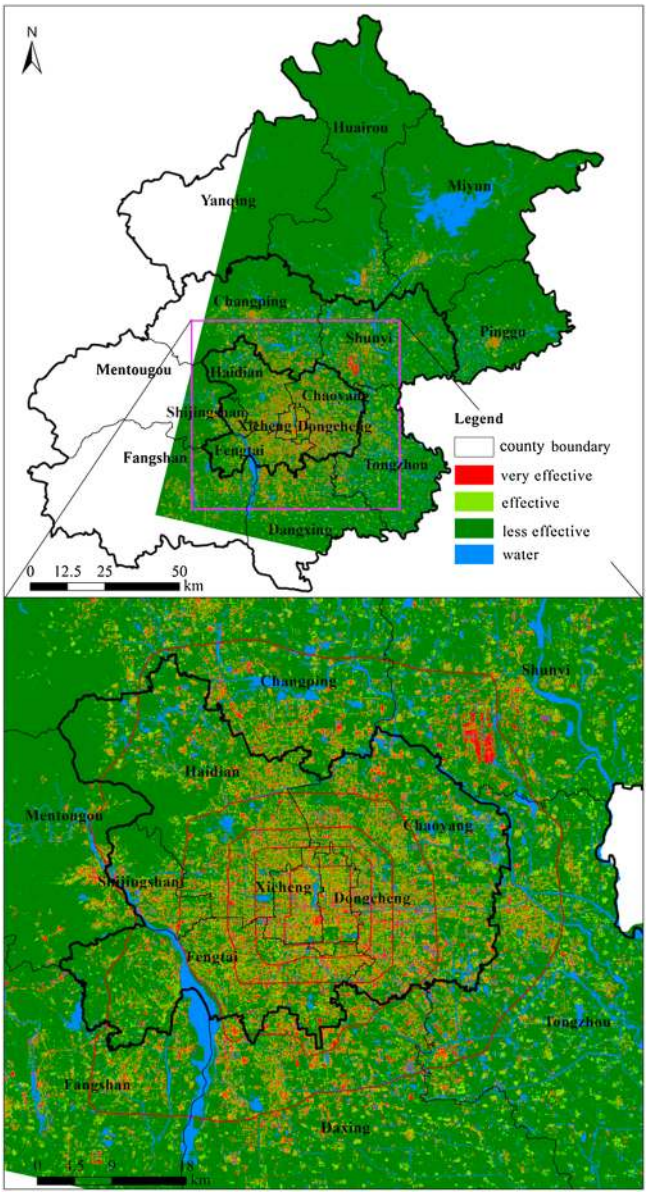

Figure 11. Areas where urban greenery project will be very effective, effective, and less effective in heat stress regulating.

2004]. According to the model simulations by *Sugawara and Takamura* [2006], our approach may result in up to 4% overestimate of summer R_{lu} in north-south oriented high-rise built-up areas where street canyon height:width ratio (H/W) equaled 1. The magnitude of error varies depending on the canyon geometry and time, with a smaller overestimates ($< 3\%$) found in east-west oriented streets or in wintertime (overestimates $<1\%$). *Sugawara and Takamura* [2006]'s study also indicated that the error would decrease with reduced H/W, reaching 1.8%–2% when $H/W = 0.5$.

To avoid the anisotropy-related error, a mechanistic model that can address the different thermal, radiative, and moisture properties of the myriad surface facets in urban was preferred [*Soux et al.*, 2004], and precise 3-D configuration of urban canopy as well as high-resolution urban climate (wind and air temperature) data sets were required as the model drivers [*Sugawara and Takamura*, 2006]. Due to the limitations in computational capacity and data availability, however, we were unable to apply such approach in this landscape-scale and multiyear study in Beijing. Nevertheless, the overestimation of R_{lu} in our current study could be much lower than 4% because of the complex orientation of the streets (many were east-west oriented) and the relative open landscape (i.e., low H/W) of Beijing. Furthermore, our study was conducted in autumn when the problem of emission anisotropy was lower than in summer [*Sugawara and Takamura*, 2006]. The anisotropy-related error was probably within the typical error in in situ heat flux measurements that was used for the model calibration/validation and might not significantly deteriorate the accuracy of our study results.

5. Conclusion

The trapezoid method, as represented by the PCACA model, avoids the necessity to quantify various surface resistance parameters that cannot be estimated remote sensingly and is more practical for urban heat flux study. However, previous studies were unable to quantify the PCACA model parameters. Their empirical approach to determine the trapezoid boundary often leads to uncertainties because of subjective judgment. We altered the formula of the PCACA algorithm and calibrated the model with synchronously measured Bowen ratios by nonlinear fitting. This approach is more accurate and suitable for urban heat flux mapping.

The land surface temperature (i.e., LST), H, and β of the Beijing metropolitan area were found to increase along the outskirt-suburban-urban gradient, with strong spatial variation. The northern city has a lower LST, H, and β than the southern city. Furthermore, the heat fluxes differed significantly among different urban land use types. For example, the Bowen ratio was higher in airport and central business district compared with the residential areas and urban parks. Notably, we found that the Bowen ratio of modern high-rise residential areas was lower than that of traditional low-rise residential areas, possibly due to its higher proportion of green spaces and shaded land surface. For the purpose of heat stress regulation, it is recommendable to upgrade the traditional low-rise residential areas to modern high-rise residential areas that have lower sensible heat and preserve water surfaces in city center. We found that the thermal regulating strength of vegetation (LE/VFC) decreased exponentially with increased green space coverage and recommend the municipal administrator to focus on expanding the green spaces in intensively built-up areas like the city center and the southern part of built-up area.

Acknowledgments

This work was supported primarily by the National Natural Science Foundation of China (41371408), the National Science Foundation of China under the grant 31170347, the National Basic Research Program of China (2010CB950900, 2014CB954302), and the National Key Technology R&D Program (2012BAJ15B02). We thank S. Liu (smliu@bnu.edu.cn) from Beijing Normal University, Beijing Urban Ecology Research Station (http://www.bjurban.rcees.cas.cn/), and the Institute of Atmospheric Physics, Chinese Academy of Sciences (http://www.iap.cas.cn/jgsz/kyjg/201208/t20120831_3636298.html), for providing the eddy covariance data sets.

References

Arnfield, A. J. (2003), Two decades of urban climate research: A review of turbulence, exchanges of energy and water, and the urban heat island, *Int. J. Climatol.*, *23*(1), 1–26, doi:10.1002/joc.859.

Asaeda, T., and V. T. Ca (1993), The subsurface transport of heat and moisture and its effect on the environment: A numerical model, *Boundary Layer Meteorol.*, *65*, 159–179, doi:10.1007/BF00708822.

Bastiaanssen, W. G. M., M. Menenti, R. A. Feddes, and A. A. M. Holtslag (1998), A remote sensing surface energy balance algorithm for land (SEBAL): 1. Formulation, *J. Hydrol.*, *212-213*, 198–212, doi:10.1016/S0022-1694(98)00253-4.

Beijing Municipal Bureau Statistics (2014), *Beijing Statistical Information Net* [in Chinese]. [Available at http://www.bjstats.gov.cn/.]

Beijing Municipal Institute of City Planning and Design (2004), *Planning on Greenland System in Beijing City* [in Chinese]. [Available at http://chy.bjghw.gov.cn.]

Buyantuyev, A., and J. Wu (2010), Urban heat islands and landscape heterogeneity: Linking spatiotemporal variations in surface temperatures to land-cover and socioeconomic patterns, *Landscape Ecol.*, *25*, 17–33.

Cao, X., A. Onishi, J. Chen, and H. Imura (2010), Quantifying the cool island intensity of urban parks using ASTER and IKONOS data, *Landscape Urban Plan.*, *96*(4), 224–231, doi:10.1016/j.landurbplan.2010.03.008.

Carlson, T. N. (2007), An overview of the "triangle method" for estimating surface evapotranspiration and soil moisture from satellite imagery, *Sensors*, *7*, 1612–1629.

Carlson, T. N., and D. A. Ripley (1997), On the relation between NDVI, fractional vegetation cover, and leaf area index, *Remote Sens. Environ.*, *62*(3), 241–252, doi:10.1016/S0034-4257(97)00104-1.

Carlson, T. N., R. R. Gillies, and T. J. Schmugge (1995), An interpretation of methodologies for indirect measurement of soil-water content, *Agric. For. Meteorol.*, *77*, 191–205, doi:10.1016/0168-1923(95)02261-U.

Chen, B., G. Shi, B. Wang, J. Zhao, and S. Tan (2012), Estimation of the anthropogenic heat release distribution in China from 1992 to 2009, *Acta Meteorol. Sin.*, *26*(4), 507–515, doi:10.1007/s13351-012-0409-y.

Chen, W. Y. (2006), Assessing the services and value of green spaces in urban ecosystem: A case of Guangzhou City, PhD thesis, Univ. of Hong Kong, Hong Kong.

Chen, Z., X. Su, S. Liu, R. Gu, and Y. Li (1998), A study of ecological benefits of urban forests in Beijing (2) [in Chinese], *J. Chin. Landscape Archit 14*(2), 51–53.

Choudhury, B. J. (1989), Estimating evaporation and carbon assimilation using infrared temperature data: Vistas in modeling, in *Theory and Applications of Optical Remote Sensing*, edited by G. Asrar, pp. 628–690, John Wiley, New York.

Cui, Y. P., J. Y. Liu, Y. F. Hu, J. B. Wang, and W. H. Kuang (2012), Modeling the radiation balance of different urban underlying surfaces, *Chin. Sci. Bull.*, *57*(8), 1046–1054, doi:10.1007/s11434-011-4933-x.

Goetz, S. J. (1997), Multi-sensor analysis of NDVI, surface temperature and biophysical variables at a mixed grassland site, *Int. J. Remote Sens.*, *18*(1), 71–94, doi:10.1080/014311697219286.

Goldbach, A., and W. Kuttler (2013), Quantification of turbulent heat fluxes for adaptation strategies within urban planning, *Int. J. Climatol.*, *33*(1), 143–159, doi:10.1002/joc.3437.

Grimm, N. B., S. H. Faeth, N. E. Golubiewski, C. L. Redman, J. Wu, X. Bai, and J. M. Briggs (2008), Global change and the ecology of cities, *Science*, *319*(5864), 756–760, doi:10.1126/science.1150195.

Grimmond, C. S. B. (2005), Progress in measuring and observing the urban atmosphere, *Theor. Appl. Climatol.*, *84*(1-3), 3–22, doi:10.1007/s00704-005-0140-5.

Grimmond, C. S. B., T. S. King, F. D. Cropley, D. J. Nowak, and C. Souch (2002), Local-scale fluxes of carbon dioxide in urban environments: Methodological challenges and results from Chicago, *Environ. Pollut.*, *116*, S243–S254, doi:10.1016/S0269-7491(01)00256-1.

Grimmond, S. (2007), Urbanization and global environmental change: Local effects of urban warming, *Geogr. J.*, *173*(1), 83–88, doi:10.1111/j.1475-4959.2007.232_3.x.

Gutman, G., and A. Ignatov (1998), The derivation of the green vegetation fraction from NOAA/AVHRR data for use in numerical weather prediction models, *Int. J. Remote Sens.*, *19*(8), 1533–1543.

Imhoff, M. L., P. Zhang, R. E. Wolfe, and L. Bounoua (2010), Remote sensing of the urban heat island effect across biomes in the continental USA, *Remote Sens. Environ.*, *114*(3), 504–513, doi:10.1016/j.rse.2009.10.008.

Jenerette, G. D., S. L. Harlan, W. L. Stefanov, and C. A. Martin (2011), Ecosystem services and urban heat riskscape moderation: Water, green spaces, and social inequality in Phoenix, USA, *Ecol. Appl.*, *21*, 2637–2651, doi:10.1890/10-1493.1.

Jia, Z. Z., S. M. Liu, Z. W. Xu, Y. J. Chen, and M. J. Zhu (2012), Validation of remotely sensed evapotranspiration over the Hai River Basin, China, *J. Geophys. Res.*, *117*, D13113, doi:10.1029/2011JD017037.

Jiang, Z., A. R. Huete, J. Chen, Y. Chen, J. Li, G. Yan, and X. Zhang (2006), Analysis of NDVI and scaled difference vegetation index retrievals of vegetation fraction, *Remote Sens. Environ.*, *101*(3), 366–378, doi:10.1016/j.rse.2006.01.003.

Jim, C. Y., and W. Y. Chen (2009), Ecosystem services and valuation of urban forests in China, *Cities*, *26*, 187–194, doi:10.1016/j.cities.2009.03.003.
Johnson, G. T., and I. D. Watson (1984), The determination of view-factors in urban canyons, *J. Climate Appl. Meteorol.*, *23*, 329–335.
Kalnay, E., and M. Cai (2003), Impact of urbanization and land-use change on climate, *Nature*, *423*(6939), 528–531, doi:10.1038/nature01675.
Ke, X. L., J. Y. Zhan, E. J. Ma, and J. Huang (2014), *Regional Climate Impacts of Future Urbanization in China*, 167–206, Springer Geography, Springer, Berlin, doi:10.1007/978-3-642-54876-5_6.
Kuang, W. (2011), Simulating dynamic urban expansion at regional scale in Beijing-Tianjin-Tangshan Metropolitan Area, *J. Geogr Sci.*, *21*(2), 317–330, doi:10.1007/s11442-011-0847-4.
Kuang, W. (2012a), Evaluating impervious surface growth and its impacts on water environment in Beijing-Tianjin-Tangshan Metropolitan Area, *J. Geogr Sci.*, *22*(3), 535–547, doi:10.1007/s11442-012-0945-y.
Kuang, W. (2012b), Spatio-temporal patterns of intra-urban land use change in Beijing, China between 1984 and 2008, *Chin. Geogr. Sci.*, *22*(2), 210–220, doi:10.1007/s11769-012-0529-x.
Kuang, W., J. Liu, Z. Zhang, D. Lu, and B. Xiang (2013), Spatiotemporal dynamics of impervious surface areas across China during the early 21st century, *Chin. Sci. Bull.*, *58*(14), 1691–1701, doi:10.1007/s11434-012-5568-2.
Laaidi, K., A. Zeghnoun, B. Dousset, P. Bretin, S. Vandentorren, E. Giraudet, and P. Beaudeau (2012), The impact of heat islands on mortality in Paris during the August 2003 heat wave, *Environ. Health Persp.*, *120*(2), 254–259, doi:10.1289/ehp.1103532.
Leprieur, C., Y. H. Kerr, S. Mastorchio, and J. C. Meunier (2000), Monitoring vegetation cover across semi-arid regions: Comparison of remote observations from various scales, *Int. J. Remote Sens.*, *21*(2), 281–300, doi:10.1080/014311600210830.
Li, F., W. T. Crowa, and W. P. Kustas (2010), Towards the estimation root-zone soil moisture via the simultaneous assimilation of thermal and microwave soil moisture retrievals, *Adv. Water Resour.*, *33*, 201–204, doi:10.1016/j.advwatres.2009.11.007.
Li, Z. L., B. H. Tang, H. Wu, H. Ren, G. Yan, Z. Wan, I. F. Trigo, and J. A. Sobrino (2013), Satellite-derived land surface temperature: Current status and perspectives, *Remote Sens. Environ.*, *131*, 14–37, doi:10.1016/j.rse.2012.12.008.
Liu, H. Z., J. W. Feng, L. Järvi, and T. Vesala (2012a), Eddy covariance measurements of CO_2 and energy fluxes in the city of Beijing, *Atmos. Chem. Phys. Discuss.*, *12*(3), 7677–7704, doi:10.5194/acpd-12-7677-2012.
Liu, H. Z., J. W. Feng, L. Järvi, and T. Vesala (2012b), Four-year (2006-2009) eddy covariance measurements of CO_2 flux over an urban area in Beijing, *Atmos. Chem. Phys.*, *12*(17), 7881–7892, doi:10.5194/acp-12-7881-2012.
Liu, S. M., Z. W. Xu, Z. L. Zhu, Z. Z. Jia, and M. J. Zhu (2013), Measurements of evapotranspiration from eddy-covariance systems and large aperture scintillometers in the Hai River Basin, China, *J. Hydrol.*, *487*, 24–38, doi:10.1016/j.jhydrol.2013.02.025.
Liu, Y., G. Shintaro, D. F. Zhuang, and W. H. Kuang (2012), Urban surface heat fluxes infrared remote sensing inversion and their relationship with land use types, *J. Geogr. Sci.*, *22*(4), 699–715, doi:10.1007/s11442-012-0957-7.
Mallick, J., A. Rahman, and C. K. Singh (2013), Modeling urban heat islands in heterogeneous land surface and its correlation with impervious surface area by using night-time ASTER satellite data in highly urbanizing city, Delhi-India, *Adv. Space Res.*, *52*(4), 639–655, doi:10.1016/j.asr.2013.04.025.
Markham, B. L., and J. L. Barker (1987), Thematic Mapper band pass solar exoatmospheric irradiances, *Int. J. Remote Sens.*, *8*, 517–523, doi:10.1080/01431168708948658.
Miao, S., J. Dou, F. Chen, J. Li, and A. Li (2012), Analysis of observations on the urban surface energy balance in Beijing, *Sci. China Earth Sci.*, *55*(11), 1881–1890, doi:10.1007/s11430-012-4411-6.
Mirzaei, P. A., and F. Haghighat (2010), Approaches to study urban heat island–abilities and limitations, *Build Environ*, *45*(10), 2192–2201, doi:10.1016/j.buildenv.2010.04.001.
Moran, M. S., R. D. Jackson, L. H. Raymond, L. W. Gay, and P. N. Slater (1989), Mapping surface energy balance components by combining Landsat Thematic Mapper and ground-based meteorological data, *Remote Sens. Environ.*, *30*(1), 77–87, doi:10.1016/0034-4257(89)90049-7.
Niemelä, S., P. Räisänen, and H. Savijä (2001a), Comparison of surface radiative flux parameterizations: Part II: Shortwave radiation, *Atmos. Res.*, *58*, 141–154, doi:10.1016/S0169-8095(01)00085-0.
Niemelä, S., P. Räisänen, and H. Savijä (2001b), Comparision of surface radiative flux parameterizations: PartI: Longwave radiation, *Atmos.Res.*, *58*, 1–8, doi:10.1016/S0169-8095(01)00084-9.
Norman, J. M., W. P. Kustas, and K. S. Humes (1995), A two-source approach for estimating soil and vegetation energy fluxes in observations of directional radiometric surface temperature, *Agric. For. Meteorol*, *77*, 263–293.
Offerle, B., C. S. B. Grimmond, and T. R. Oke (2003), Parameterization of net all-wave radiation for urban areas, *J. Appl. Meteorol.*, *42*, 1157–1173, doi:10.1175/1520-0450(2003)042<1157:PONARF>2.0.CO;2.
Oke, T. R. (1979), Advectively-assisted evapotranspiration from irrigated urban vegetation, *Boundary Layer Meteorol.*, *17*, 167–173, doi:10.1007/BF00117976.
Oke, T. R. (1982), The energetic basis of the urban heat island, *Quart. J. R. Met. Soc.*, *108*(455), 1–24, doi:10.1002/qj.49710845502.
Owen, T., T. Carlson, and R. Gillies (1998), An assessment of satellite remotely-sensed land cover parameters in quantitatively describing the climatic effect of urbanization, *Int. J. Remote Sens.*, *19*(9), 1663–1681, doi:10.1080/014311698215171.
Pu, R., P. Gong, R. Michishita, and T. Sasagawa (2006), Assessment of multi-resolution and multi-sensor data for urban surface temperature retrieval, *Remote Sens. Environ.*, *104*, 211–225.
Qin, Z., A. Karnieli, and P. Berliner (2001), A mono-window algorithm for retrieving land surface temperature from Landsat TM data and its application to the Israel-Egypt border region, *Int. J. Remote Sens.*, *22*(18), 3719–3746, doi:10.1080/01431160010006971.
Schmid, H. P., H. A. Cleugh, C. S. B. Grimmond, and T. R. Oke (1991), Spatial variability of energy fluxes in suburban terrain, *Boundary Layer Meteorol.*, *54*(3), 249–276, doi:10.1007/BF00183956.
Seto, K. C., B. Güneralp, and L. R. Hutyra (2012), Global forecasts of urban expansion to 2030 and direct impacts on biodiversity and carbon pools, *Proc. Natl. Acad. Sci. U.S.A.*, *109*(40), 16,083–16,088, doi:10.1073/pnas.1211658109.
Sobrino, J. A., J. C. Jiménez-Muñoz, and L. Paolini (2004), Land surface temperature retrieval from Landsat TM5, *Remote Sens. Environ.*, *90*(4), 434–440, doi:10.1016/j.rse.2004.02.003.
Soux, A., J. A. Voogt, and T. R. Oke (2004), A model to calculate what a remote sensor 'sees' of an urban surface, *Boundary Layer Meteorol.*, *111*, 109–132.
Spronken-Smith, R. A., T. R. Oke, and W. P. Lowry (2000), Advection and the surface energy balance across an irrigated urban park, *Int. J. Climatol.*, *20*, 1033–1047, doi:10.1002/1097-0088(200007)20:9<1033::AID-JOC508>3.0.CO;2-U.
Stone, B. (2009), Land use as climate change mitigation, *Environ. Sci. Technol.*, *43*, 9052–9056, doi:10.1021/es902150g.
Su, H., M. F. McCabe, E. F. Wood, Z. Su, and J. H. Prueger (2005), Modeling evapotranspiration during SMACEX: Comparing two approaches for local- and regional-scale prediction, *J. Hydrometeor.*, *6*, 910–922, doi:10.1175/JHM466.1.

Su, Z. B. (2002), The Surface Energy Balance System (SEBS) for estimation of turbulent heat fluxes, *Hydrol. Earth Syst. Sci., 6*(1), 85–100, doi:10.5194/hess-6-85-2002.

Suckling, P. W. (1980), The energy balance microclimate of a suburban lawn, *J. Appl. Meteorol.*, *19*, 606–608, doi:10.1175/1520-0450(1980)019<0606:TEBMOA>2.0.CO;2.

Sugawara, H., and T. Takamura (2006), Longwave radiation flux from an urban canopy: Evaluation via measurements of directional radiometric temperature, *Remote Sens. Environ.*, *104*(2), 226–237, doi:10.1016/j.rse.2006.01.024.

Suleiman, A., and R. Crago (2002), Analytical land–atmosphere radiometer model, *J. Appl. Meteorol.*, *41*, 177–187.

Sun, W. X., M. Y. Du, and G. Y. Cai (2011), Dynamic RS monitoring and analysis of the thermal environments in Beijing urban area and the Olympic Park [in Chinese with English abstract], *Sci. Surv. Map., 36*(5), 103–105.

Vandentorren, S., P. Bretin, A. Zeghnoun, L. Mandereau-Bruno, A. Croisier, C. Cochet, J. Ribéron, I. Siberan, B. Declercq, and M. Ledrans (2006), August 2003 heat wave in France: Risk factors for death of elderly people living at home, *Eur. J. Public Health*, *16*(6), 583–591, doi:10.1093/eurpub/ckl063.

Verhoef, A., H. A. R. De Bruin, and B. J. J. M. Van Den Hurk (1997), Some practical notes on the parameter kB^{-1} for sparse vegetation, *J. Appl. Meteorol.*, *36*, 560–572, doi:10.1175/1520-0450(1997)036<0560:SPNOTP>2.0.CO;2.

Voogt, J. A., and C. S. B. Grimmond (2000), Modeling surface sensible heat flux using surface radiative temperatures in a simple urban area, *J. Appl. Meteorol.*, *39*(10), 1679–1699, doi:10.1175/1520-0450-39.10.1679.

Voogt, J. A., and T. Oke (1998), Effects of urban surface geometry on remotely-sensed surface temperature, *Int. J. Remote Sens.*, *19*, 895–920.

Wang, K., J. Wang, P. Wang, M. Sparrow, J. Yang, and H. Chen (2007), Influences of urbanization on surface characteristics as derived from the moderate-resolution imaging spectroradiometer: A case study for the Beijing metropolitan area, *J. Geophys. Res.*, *112*, D22S06, doi:10.1029/2006JD007997.

Wang, X. X., et al. (2007), Analysis of water, heat and CO2 fluxes on urban green space, *Acta Ecol. Sin.*, *27*(8), 3232–3239.

Wang, Y., and F. Hu (2006), Variations of the urban heat island in summer of the recent 10 years over Beijing and its environment effects [in Chinese with English abstract], *Chin. J. Geophysics*, *49*(1), 59–67, doi:10.1002/cjg2.812.

Weng, Q., and D. Lu (2008), A sub-pixel analysis of urbanization effect on land surface temperature and its interplay with impervious surface and vegetation coverage in Indianapolis, United States, *Int. J. Appl. Earth Obs. Geoinf.*, *10*(1), 68–83, doi:10.1016/j.jag.2007.05.002.

Xiao, R., Z. Ouyang, H. Zheng, W. Li, E. W. Schienke, and X. Wang (2007), Spatial pattern of impervious surfaces and their impacts on land surface temperature in Beijing, China, *J. Environ. Sci.*, *19*(2), 250–256, doi:10.1016/s1001-0742(07)60041-2.

Xiao, R., Q. Weng, Z. Ouyang, W. Li, E. W. Schienke, and Z. Zhang (2008), Land surface temperature variation and major factors in Beijing, China, *Photogramm. Eng. Remote Sens.*, *74*(4), 451–461.

Xie, Z., and H. X. Cao (1996), Asymmetric changes in maximum and minimum temperature in Beijing, *Theor. Appl. Climatol.*, *55*(1-4), 151–156, doi:10.1007/BF00864710.

Xu, W., M. J. Wooster, and C. S. B. Grimmond (2008), Modelling of urban sensible heat flux at multiple spatial scales: A demonstration using airborne hyperspectral imagery of Shanghai and a temperature-emissivity separation approach, *Remote Sens. Environ.*, *112*(9), 3493–3510, doi:10.1016/j.rse.2008.04.009.

Yan, Z., Z. Li, Q. Li, and P. Jones (2010), Effects of site change and urbanisation in the Beijing temperature series 1977-2006, *Int. J. Climatol.*, *30*, 1226–1234, doi:10.1002/joc.1971.

Yu, M., Y. Liu, Y. Dai, and A. Yang (2013), Impact of urbanization on boundary layer structure in Beijing, *Clim. Change*, *120*(1-2), 123–136, doi:10.1007/s10584-013-0788-2.

Yuan, F., and M. E. Bauer (2007), Comparison of impervious surface area and normalized difference vegetation index as indicators of surface urban heat island effects in Landsat imagery, *Remote Sens. Environ.*, *106*(3), 375–386, doi:10.1016/j.rse.2006.09.003.

Zhan, J. Y., H. Juan, T. Zhao, X. L. Geng, and Y. H. Xiong (2013), Modeling the impacts of urbanization on regional climate change: A case study in the Beijing-Tianjin-Tangshan metropolitan area, *Adv. Meteorol.*, *2013*, 1–8, doi:10.1155/2013/849479.

Zhang, C. L., F. Chen, S. G. Miao, Q. C. Li, X. A. Xia, and C. Y. Xuan (2009), Impacts of urban expansion and future green planting on summer precipitation in the Beijing metropolitan area, *J. Geophys. Res.*, *114*, D02116, doi:10.1029/2008JD010328.

Zhang, R. (2005), An operational two-layer remote sensing model to estimate surface flux in regional scale: Physical background, *Sci. China, Ser. D Earth Sci.*, *48*, doi:10.1360/05zd0023.

Zhang, R., J. Tian, H. Su, X. Sun, S. Chen, and J. Xia (2008), Two improvements of an operational two-layer model for terrestrial surface heat flux retrieval, *Sensors*, *8*(10), 6165–6187, doi:10.3390/s8106165.

Zhang, W., F. Zhang, Z. Yan, and Z. Zhang (2006), Initial analysis on the ecological service value of the greening land in Lanzhou city [in Chinese with English abstract], *Pratacult. Sci.*, *23*(11), 98–102.

Zhang, X. X., P. F. Wu, and B. Chen (2010), Relationship between vegetation greenness and urban heat island effect in Beijing City of China, *Procedia Environ. Sci.*, *2*, 1438–1450, doi:10.1016/j.proenv.2010.10.157.

Zhang, Y., I. O. A. Odeh, and C. Han (2009), Bi-temporal characterization of land surface temperature in relation to impervious surface area, NDVI and NDBI, using a sub-pixel image analysis, *Int. J. Appl. Earth Obs. Geoinf.*, *11*(4), 256–264, doi:10.1016/j.jag.2009.03.001.